

Supplementary Information

Fe-MIL-101 Metal Organic Framework Enhanced Solid Polymer Electrolytes for High-Performance Solid-State Lithium Metal Batteries

Ramesh Subramani,^{a,‡} Su-Yang Hsu,^{a,‡} Yu-Chun Chuang,^a Liang-Ching Hsu,^a Kueih-Tzu Lu,^{a,*} Jin-Ming Chen^{a,b,*}

^aNational Synchrotron Radiation Research Center, Hsinchu, 30076, Taiwan.

^bDepartment of Electrophysics, National Yang Ming Chiao Tung University (NYCU), Hsinchu 30010, Taiwan

* Corresponding Author (E-mail: ktlu@nsrrc.org.tw) (K. T. L)

* Corresponding Author (E-mail: jmchen@nsrrc.org.tw) (J. M. C.)

‡ The authors contributed equally to this work.

Keywords: solid polymer electrolytes, Fe-MIL-101, MOF fillers, *in-situ* XRD, XAS, solid-state LMBs

Supplementary Information for:

- (1) Crystal structure of Fe-MIL-101
- (2) SEM and EDS mappings of Fe-MIL-101 powder
- (3) XRD profiles of Fe-MIL-101, PVdF-HFP, and SPE-10 membrane
- (4) Cross-sectional SEM image of Fe-MIL-101-integrated SPE membrane
- (5) Optical image, SEM and EDS of SPE-0
- (6) EIS spectra of various SPEs at different temperatures
- (7) t_{Li^+} measurements of different SPEs
- (8) EIS of Li||Li symmetric cells
- (9) DSC curves of SPE-0 and SPE-10 membranes
- (10) Plating-stripping profile of Li|SPE|Li symmetric cells
- (11) Tafel plots of Li|SPE|Li symmetric cells
- (12) RDF of FT k^3 -weighted Fe K-edge EXAFS spectra of Fe- MIL-101 and SPE-10
- (13) CV profiles of Li|SPE-10|LFP and Li|SPE-0|LFP cells
- (14) EIS profiles of Li|SPE-10|LFP and Li|SPE-0|LFP cells
- (15) Comparison of electrochemical performance of solid-state Li||LFP batteries
- (16) XRD patterns of the LFP cathodes
- (17) Fe K-edge XANES and RDF of FT k^3 -weighted EXAFS spectra of Li|SPE-0|LFP cells
- (18) *In-situ* Li|SPE-10|LFP cell
- (19) *In-situ* XRD patterns of Li|SPE-10|LFP cell
- (20) Rate capability of Li|SPE-0|NMC622 cell

1. Crystal structure of Fe-MIL-101

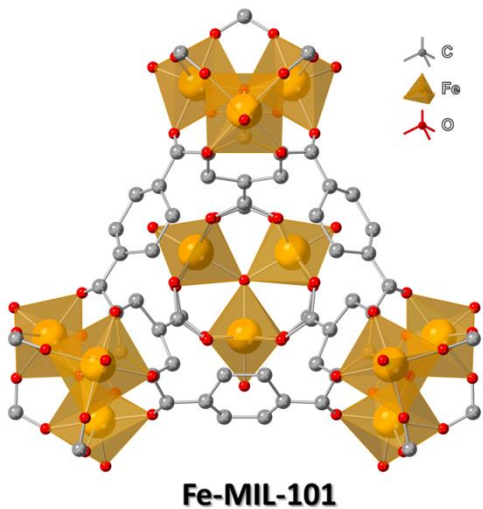


Fig. S1 Crystal structure of Fe-MIL-101.

2. SEM and EDS mappings of Fe-MIL-101 powder

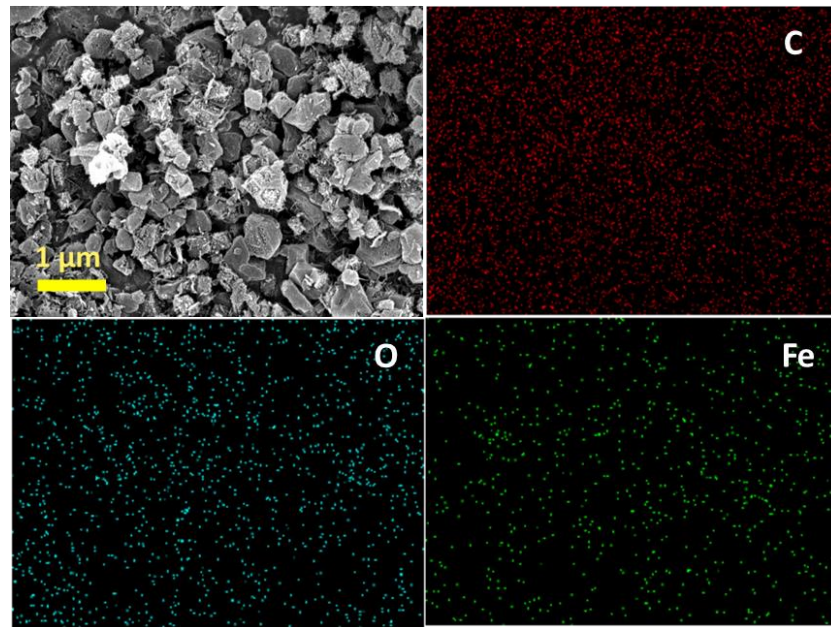


Fig. S2 SEM image of Fe-MIL-101 powder with corresponding elemental mapping.

3. XRD profiles of Fe-MIL-101, PVdF-HFP, and SPE-10 membrane

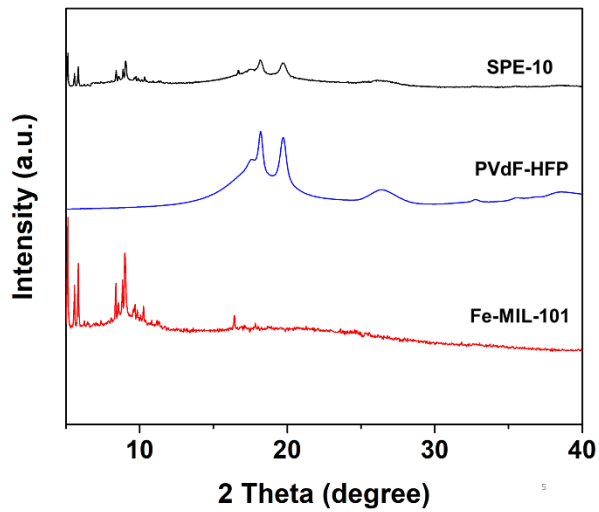


Fig. S3 XRD profiles of Fe-MIL-101, PVdF-HFP, and SPE-10 membrane.

4. Cross-sectional SEM image of Fe-MIL-101-integrated SPE membrane

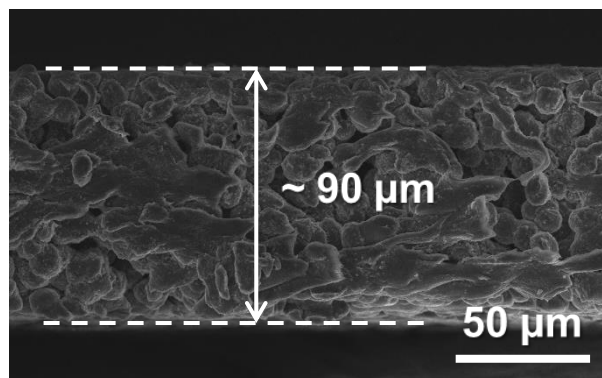


Fig. S4 Cross-sectional SEM image of Fe-MIL-101-integrated SPE membrane.

5. Optical image, SEM and EDS of SPE-0

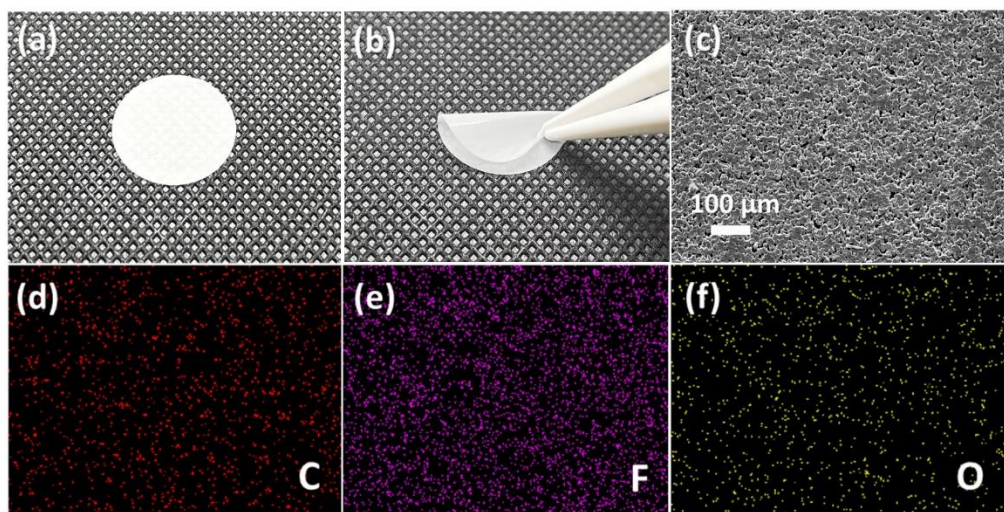


Fig. S5 Characterization of SPE membrane without Fe-MIL-101 (SPE-0): a) Optical image of SPE-0; b) Optical image of folded SPE-0; c) Top-view SEM image; and d, e, f) the corresponding elemental mappings of SPE-0.

6. EIS spectra of various SPEs at different temperatures

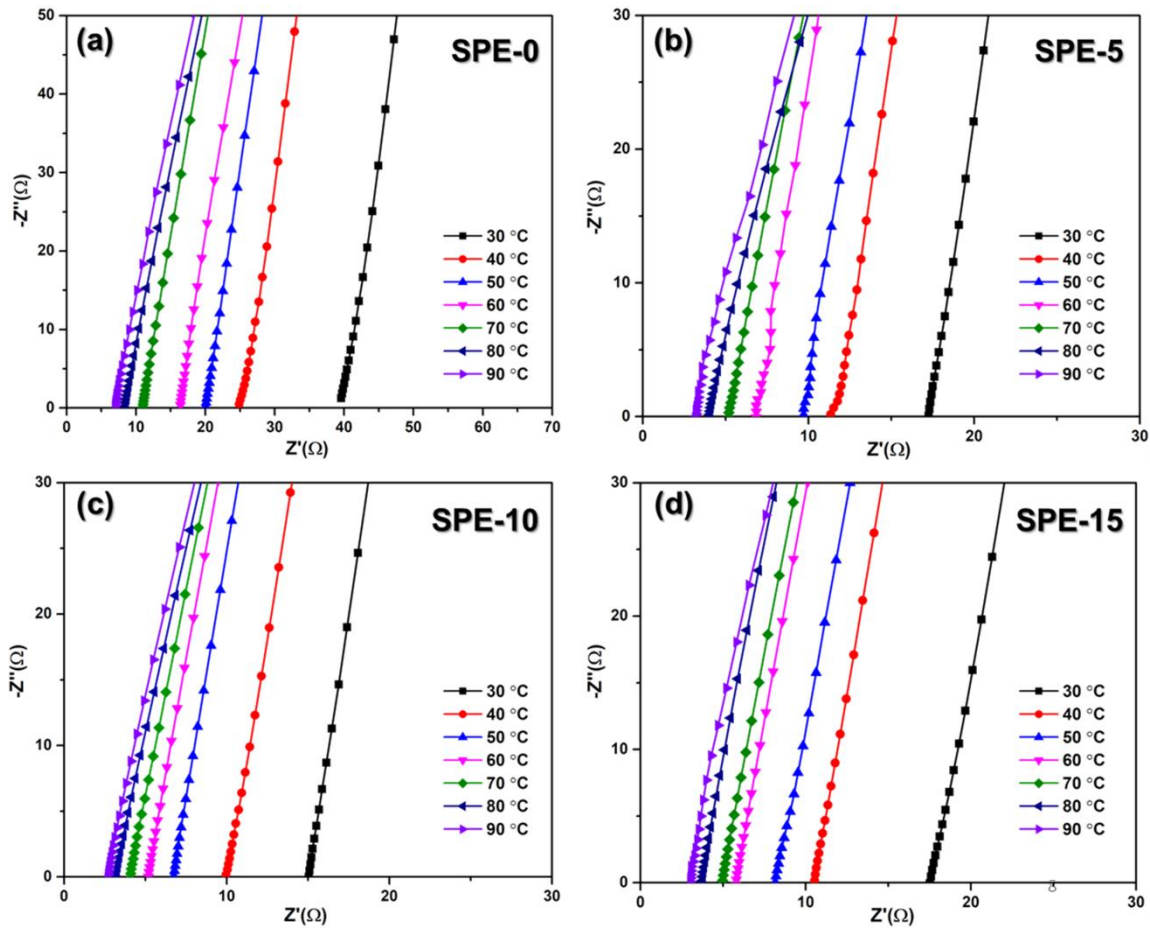


Fig. S6 EIS spectra of various SPEs at different temperatures ranging from 30 to 90 $^{\circ}\text{C}$: a) SPE-0, b) SPE-5, c) SPE-10 and d) SPE-15.

7. t_{Li^+} measurements of different SPEs

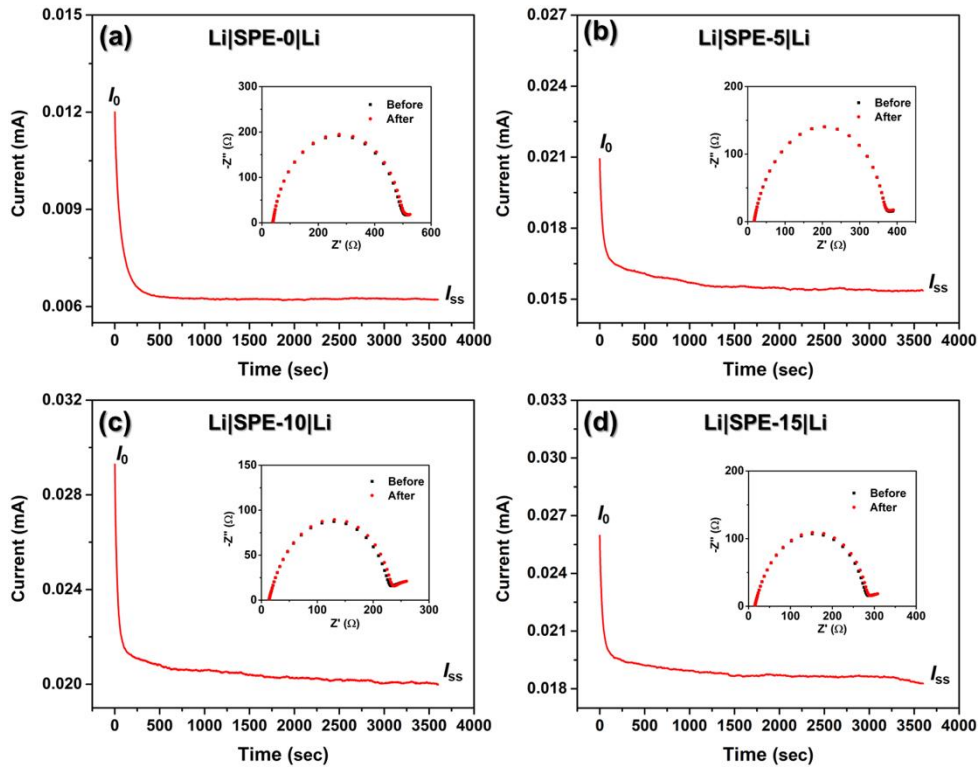


Fig. S7 a-d) Chronoamperometry curves of $\text{Li}||\text{Li}$ symmetric cells under 10 mV polarization with SPE-0, SPE-5, SPE-10, and SPE-15 electrolytes, respectively. Insets of Fig. S7a, b, c, and d show Nyquist profiles of the corresponding cell before and after polarization.

8. EIS of Li||Li symmetric cells

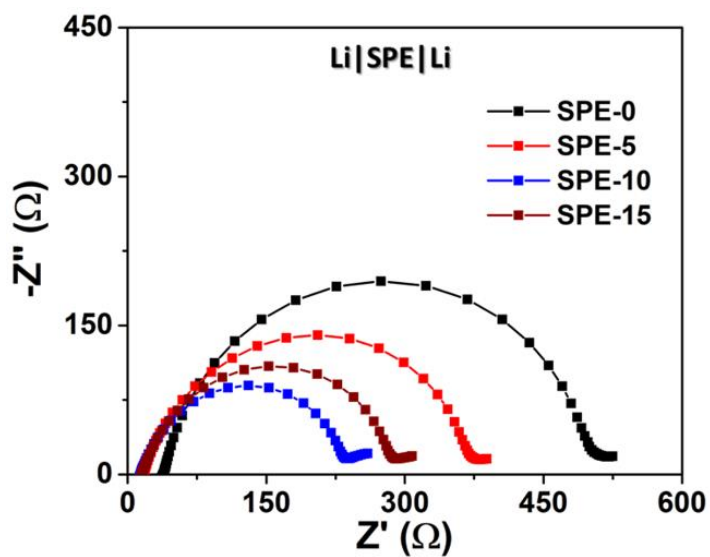


Fig. S8 Electrochemical impedance profiles of Li|SPE|Li cells with different SPEs.

9. DSC curves of SPE-0 and SPE-10 membranes

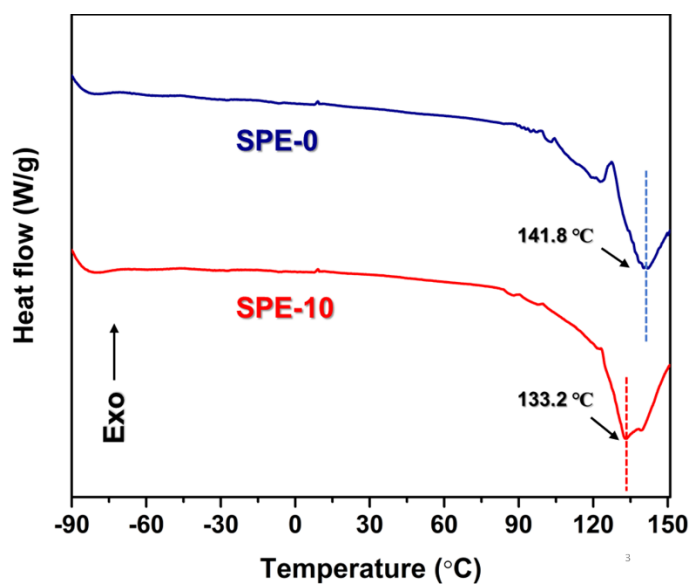


Fig. S9 DSC curves of SPE-0 and SPE-10 membranes.

10. Plating-stripping profile of Li|SPE|Li symmetric cells

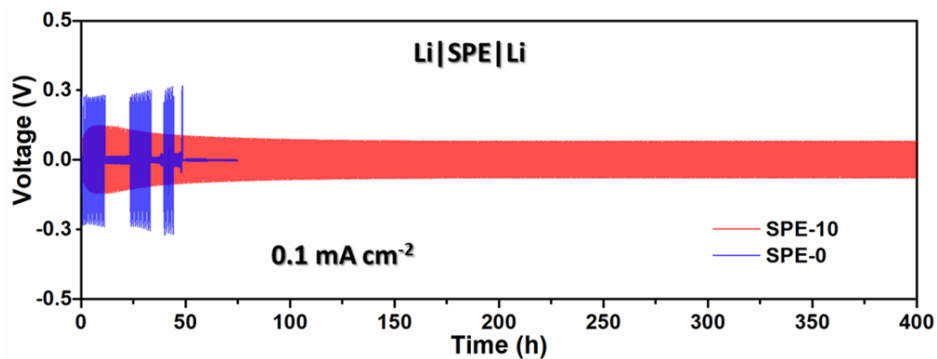


Fig. S10 Time-voltage profiles of SPE-0 and SPE-10 in a Li||Li symmetric cell at a current density of 0.1 mA cm^{-2} .

11. Tafel plots of Li|SPE|Li symmetric cells

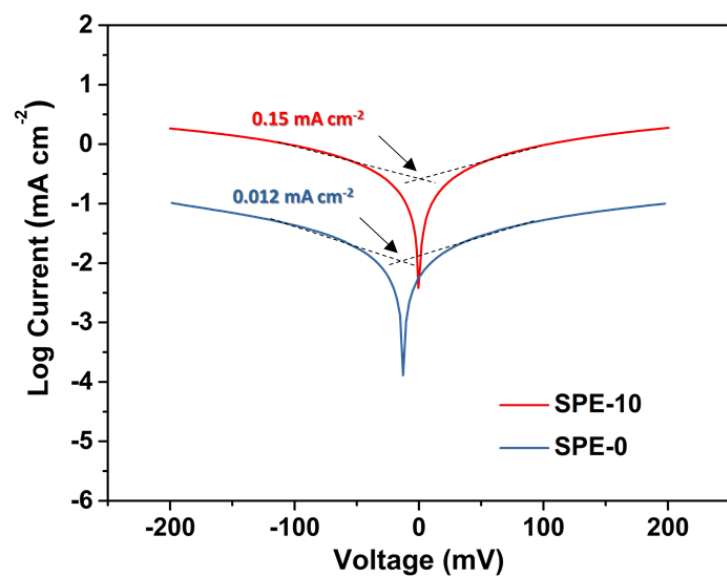


Fig. S11 Tafel plots for Li|SPE|Li symmetric cells with different SPEs.

12. RDF of FT k^3 -weighted Fe K-edge EXAFS spectra of Fe-MIL-101 and SPE-10

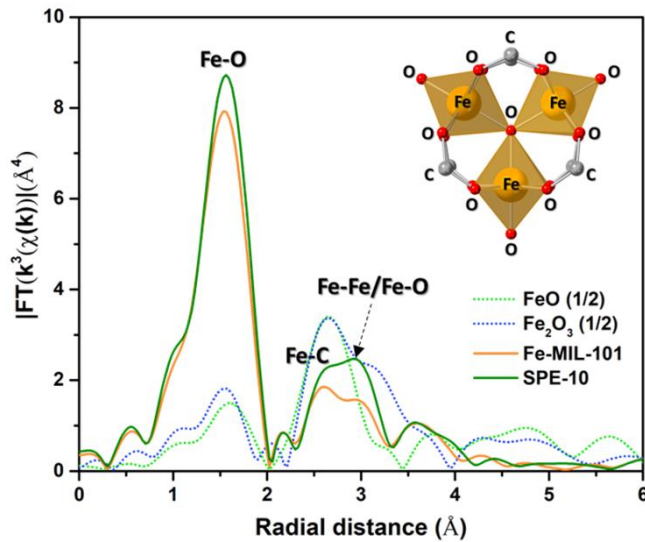


Fig. S12 RDF of FT k^3 -weighted Fe K-edge EXAFS spectra of Fe-MIL-101 and SPE-10 without phase shift correction. The intensities corresponding to FeO and Fe_2O_3 are scaled by a factor of 0.5. A fragment of Fe-MIL-101 crystal structure is shown in the inset of Fig. S12.

13. CV profiles of Li|SPE-10|LFP and Li|SPE-0|LFP cells

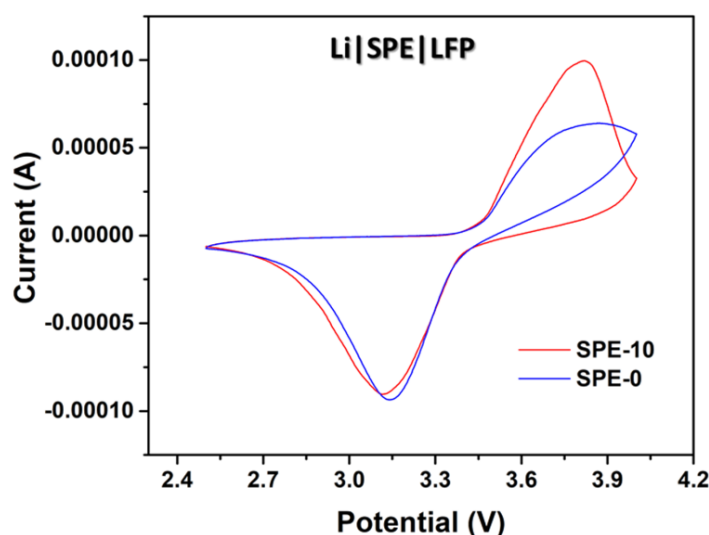


Fig. S13 CV profiles of SPE-0 and SPE-10 in a Li||LFP cell at a scan rate of 0.1 mV s^{-1} .

14. EIS of Li|SPE-10|LFP and Li|SPE-0|LFP cells

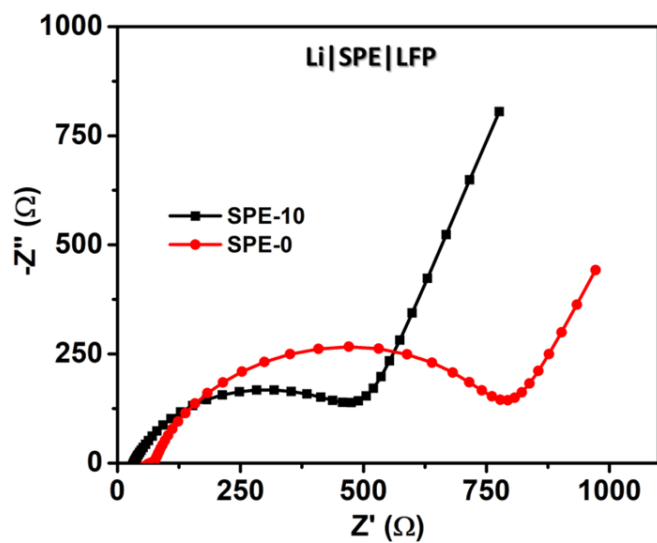


Fig. S14 Electrochemical impedance spectra of SPE-0 and SPE-10 in a Li||LFP cell.

15. Comparison of electrochemical performance of solid-state Li||LFP batteries

Polymer matrix	Fillers	Rate (C)	Capacity retention (%)	Temperature °C	Refs.
PEO/LiTFSI	Fe-MIL-100	0.2	98.2 @ 100 cycles	60	1
	PDA ^{a)} coated				
PEO/LiTFSI	hollow SiO ₂ nanosphere	0.2	97.2 @ 205 cycles	60	2
PEO/LiTFSI/EMIM-TFSI ^{b)}	Co/HPCN ^{c)}	0.2	99.1 @ 150 cycles	60	3
PEO/LiTFSI	Li _{6.25} La ₃ Zr ₂ Al _{0.25} O ₁₂	0.1	80 @ 210 cycles	50	4
PEO/LiTFSI	Halloysite nanotube	0.1	90.9 @ 100 cycles ~88 @ 300 cycles	25	5
PEO/LiTFSI	Silica nanotube	0.1	83.4 @ 100 cycles	60	6
SN ^{d)} /LiTFSI	ZIF-8 ^{e)}	0.1	87.7 @ 100 cycles	-	7
PVdF-HFP/LiTFSI	Fe-MIL-101	0.2	91 @ 300 cycles 89 @ 400 cycles	RT ^{f)}	This work

^{a)}polydopamine; ^{b)}1-ethyl-3-methylimidazolium bis(trifluoromethylsulfonyl)imide; ^{c)}MOF-derived Co-doped hollow porous carbon nanocages; ^{d)}succinonitrile; ^{e)}zeolitic imidazolate framework-8; ^{f)}room temperature.

Table S1 Comparison of electrochemical performance of solid-state Li||LFP batteries achieved by various electrolytes in previous reports.

16. XRD patterns of LFP cathodes

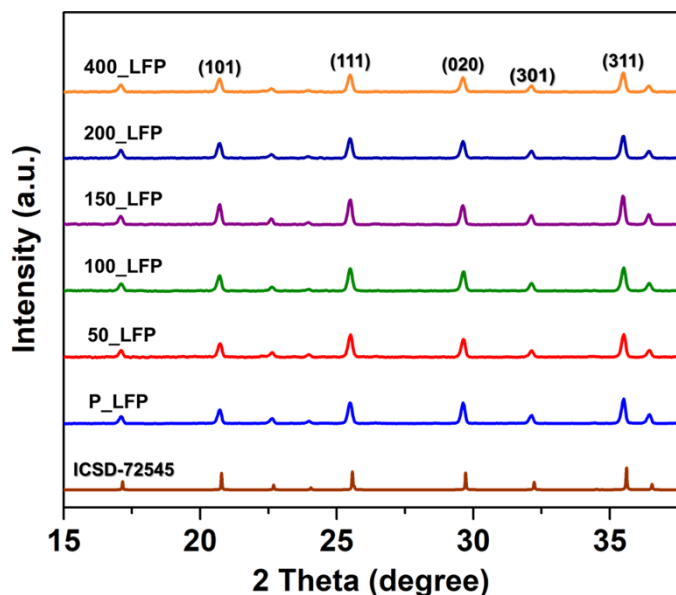


Fig. S15 XRD patterns of pristine (labeled as P_LFP) and cycled LFP cathodes detached from Li|SPE-10|LFP cells after 50, 100, 150, 200, and 400 charge-discharge cycles (labeled as 50_LFP, 100_LFP, 150_LFP, 200_LFP, and 400_LFP, respectively) at 0.2 C. 400_LFP cathode is detached from the Li|SPE-10|LFP cell used in Fig. 4e.

17. Fe K-edge XANES and RDF of FT k^3 -weighted EXAFS spectra of Li|SPE-0|LFP cells

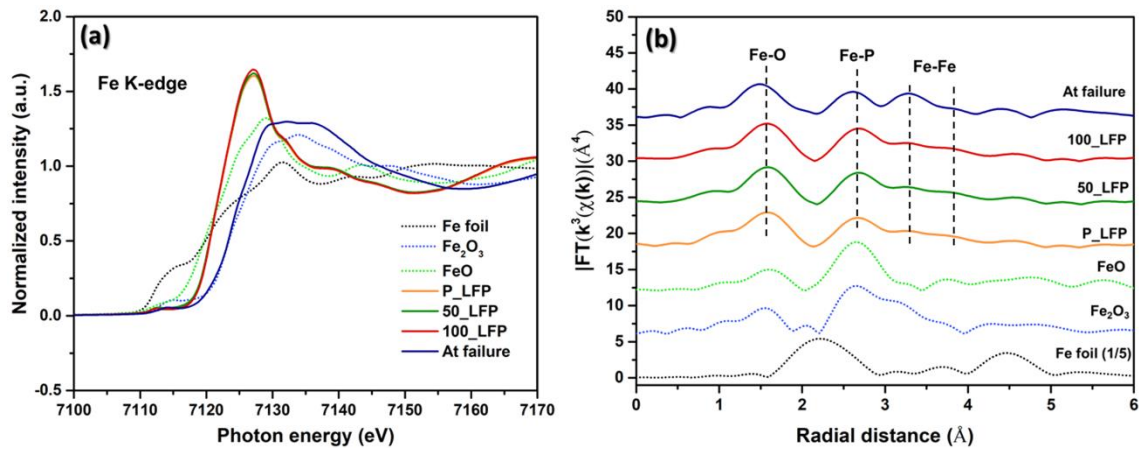


Fig. S16 a) Fe K-edge XANES, and b) RDF of FT k^3 -weighted Fe K-edge EXAFS spectra without phase shift correction of pristine (labeled as P_LFP) and cycled LFP cathodes detached from Li|SPE-0|LFP cells after 50, 100 charge-discharge cycles at 0.2 C and at failure (labeled as 50_LFP, 100_LFP, and At failure, respectively). The intensity corresponding to Fe foil in Fig. S16b is scaled by a factor of 0.2.

18. *In-situ* Li|SPE-10|LFP cell

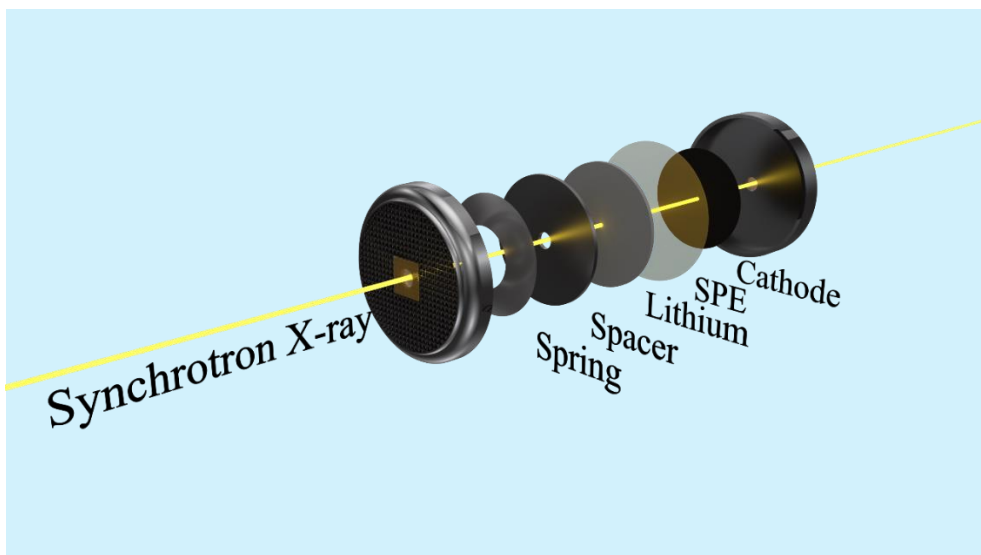


Fig. S17 *In-situ* Li|SPE-10|LFP cell.

19. *In-situ* XRD patterns of Li|SPE-10|LFP cell

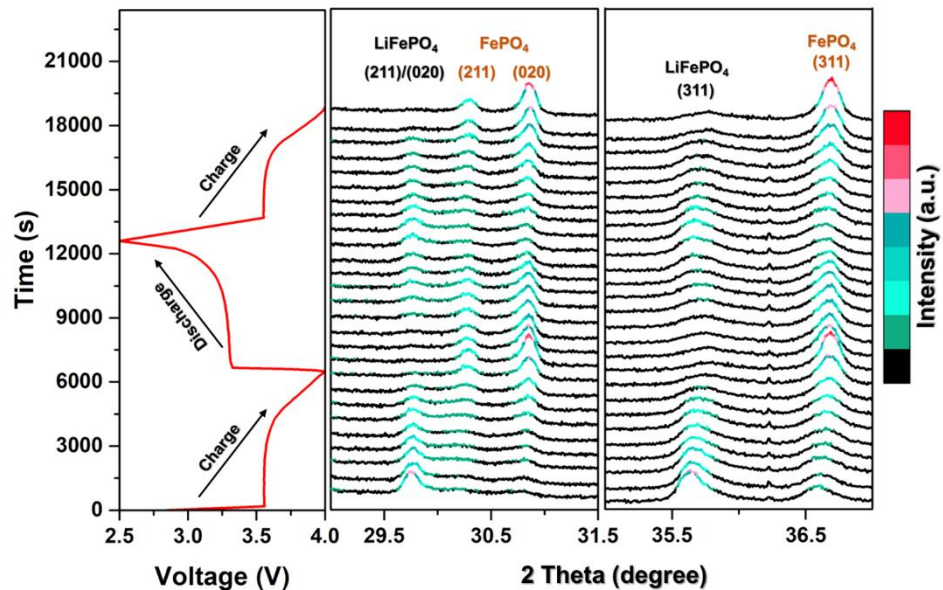


Fig. 18 XRD patterns of *in-situ* Li|SPE-10|LFP cell during the initial charge-discharge cycle at 0.2 C, along with the second charge step. The horizontal axis corresponds to specific 2-theta regions, while the vertical axis represents time. Color-coded diffraction intensity is represented, with the scale bar provided on the right side. The corresponding voltage curve is presented on the left side.

20. Rate capability of Li|SPE-0|NMC622 cell

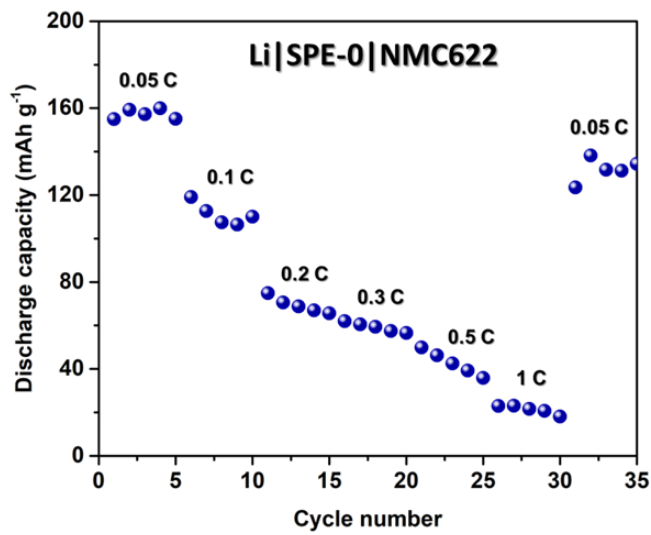


Fig. S19 Rate capability of Li|SPE-0|NMC622 cell.

References

1. T. Wei, Z. Wang, M. Zhang, Q. Zhang, J. Lu, Y. Zhou, C. Sun, Z. Yu, Y. Wang and M. Qiao, *Mater. Today Commun.*, 2022, **31**, 103518.
2. Y. Li, Y. Qin, J. Zhao, M. Ma, M. Zhang, P. Li, S. Lu, H. Bu, K. Xi and Y. Su, *ACS Appl. Mater. Interfaces*, 2022, **14**, 18360-18372.
3. Z. Zhang, Y. Huang, H. Gao, C. Li, J. Hang and P. Liu, *J. Energy Chem.*, 2021, **60**, 259-271.
4. J. Cheng, G. Hou, Q. Chen, D. Li, K. Li, Q. Yuan, J. Wang and L. Ci, *Chem. Eng. J.*, 2022, **429**, 132343.
5. Q. Zhu, X. Wang and J. D. Miller, *ACS Appl. Mater. Interfaces*, 2019, **11**, 8954-8960.
6. J. Hu, W. Wang, X. Zhu, S. Liu, Y. Wang, Y. Xu, S. Zhou, X. He and Z. Xue, *J. Membr. Sci.*, 2021, **618**, 118697.
7. D. Han, P. Wang, P. Li, J. Shi, J. Liu, P. Chen, L. Zhai, L. Mi and Y. Fu, *ACS Appl. Mater. Interfaces*, 2021, **13**, 52688-52696.